

## Critical behavior of period doublings in coupled inverted pendulums

Sang-Yoon Kim<sup>1,2,\*</sup> and Bambi Hu<sup>2,3</sup>

<sup>1</sup>*Department of Physics, Kangwon National University, Chunchon, Kangwon-Do 200-701, Korea*

<sup>2</sup>*Centre for Nonlinear Studies and Department of Physics, Hong Kong Baptist University, Hong Kong, China*

<sup>3</sup>*Department of Physics, University of Houston, Houston, Texas 77204*

(Received 13 July 1998)

We study the critical behaviors of period doublings in  $N$  ( $N=2,3,4,\dots$ ) coupled inverted pendulums by varying the driving amplitude  $A$  and the coupling strength  $c$ . It is found that the critical behaviors depend on the range of coupling interaction. In the extreme long-range case of global coupling, in which each inverted pendulum is coupled to all the other ones with equal strength, the zero-coupling critical point and an infinity of critical line segments constitute the same critical set in the  $A$ - $c$  plane, independently of  $N$ . However, for any other nonglobal-coupling cases of shorter-range couplings, the structure of the critical set becomes different from that for the global-coupling case, because of a significant change in the stability diagram of periodic orbits born via period doublings. The critical scaling behaviors on the critical set are also found to be the same as those for the abstract system of the coupled one-dimensional maps. [S1063-651X(98)05912-1]

PACS number(s): 05.45.+b, 03.20.+i, 05.70.Jk

### I. INTRODUCTION

The nonlinear dynamics of coupled nonlinear oscillators has attracted considerable attention in recent years. Such coupled oscillators are used to model many physical, chemical, and biological systems such as coupled  $p$ - $n$  junctions [1], Josephson-junction arrays [2], charge-density waves [3], chemical-reaction systems [4], and biological-oscillation systems [5]. They exhibit diverse bifurcations, multistability, chaos, pattern formation, and so on.

The coupled nonlinear oscillators studied here are coupled inverted pendulums, consisting of  $N$  identical inverted pendulums coupled through some interaction mechanism. We first consider a constituent element of the coupled dynamical system, i.e., a single parametrically forced pendulum with a vertically oscillating suspension point. It can be described by a normalized equation of motion [6],

$$\ddot{x} = f(x, \dot{x}, t) = -2\pi\beta\Omega\dot{x} - 2\pi(\Omega^2 - A\cos 2\pi t)\sin 2\pi x, \quad (1)$$

where  $x$  is a normalized angle with range  $x \in [0, 1)$ ,  $\beta$  is a normalized damping parameter,  $\Omega$  is the normalized natural frequency of the unforced pendulum, and  $A$  is the normalized driving amplitude of the vertical oscillation of the suspension point, respectively. This parametrically forced pendulum has an ‘‘inverted’’ stationary state, corresponding to the vertically up configuration with  $x = \frac{1}{2}$ . It is well known that as the parameter  $A$  is increased, the inverted pendulum undergoes a cascade of ‘‘resurrections,’’ i.e., it becomes stabilized after its instability, destabilizes again, and so forth *ad infinitum* [7–10]. Recently, we have studied bifurcations and transitions to chaos associated with such resurrections of the inverted pendulum [11]. For each case of the resurrections, the stabilized inverted state exhibits an infinite sequence of period-doubling bifurcations accumulating at a period-

doubling transition point  $A^*$ , beyond which chaos sets in. Consequently, an infinite series of period-doubling transitions to chaos occur successively with increasing  $A$ . This is in contrast to the one-dimensional (1D) map [12], where only single period-doubling transition to chaos takes place. However, the critical scaling behaviors at each  $i$ th period-doubling transition point  $A_i^*$  ( $i=1,2,3,\dots$ ) are the same as those for the 1D map.

In this paper we study the critical behaviors of period doublings in the system of  $N$  ( $N=2,3,4,\dots$ ) symmetrically coupled inverted pendulums by varying the driving amplitude  $A$  and the strength  $c$  of coupling between the inverted pendulums, and also compare them with those for the abstract system of the coupled 1D maps [13,14]. The ‘‘coupling effect’’ of the strength and range of coupling on the critical behaviors are particularly investigated. Both the structure of the critical set and the critical scaling behaviors for the coupled inverted pendulums are found to be the same as those for the coupled 1D maps found by one of us (Kim) and Kook [14].

This paper is organized as follows. We first introduce  $N$  symmetrically coupled inverted pendulums in Sec. II, and discuss their dynamical symmetries and couplings. Bifurcations associated with stability of periodic orbits and Lyapunov exponents in the coupled inverted pendulums are also discussed in Sec. III. We then investigate the critical behaviors of period doublings in the coupled inverted pendulums in Sec. IV. As in the single inverted pendulum [11], coupled inverted pendulums undergo multiple period-doubling transitions to chaos [e.g., see Figs. 2(a), 6(a), and 6(b) for the ‘‘stability trees’’ associated with the first, second, and third period-doubling transitions to chaos, respectively]. For each period-doubling transition to chaos, the critical behaviors vary depending on whether or not the coupling is global. In the extreme long-range case of global coupling, the zero-coupling critical point with  $c=0$  and an infinity of critical line segments lying on the line  $A=A_i^*$  constitute the same critical set in the  $A$ - $c$  plane, irrespectively of  $N$ . However, for any other nonglobal-coupling cases

\*Electronic address: sykim@cc.kangwon.ac.kr

of shorter-range couplings, a significant change occurs in the stability diagram of  $2^n$ -periodic ( $n=0,1,2,\dots$ ) orbits in the  $A$ - $c$  plane, and consequently the structure of the critical set becomes different from that for the global-coupling case. It is also found that the critical scaling behaviors on the critical set are the same as those for the abstract system of the coupled 1D maps [14]. Finally, a summary is given in Sec. V.

## II. SYMMETRIES AND COUPLINGS IN THE COUPLED INVERTED PENDULUMS

In this section we introduce  $N$  symmetrically coupled inverted pendulums and then discuss their symmetries and couplings. Consider  $N$  symmetrically coupled inverted pendulums with a periodic boundary condition

$$\ddot{x}_m = f(x_m, \dot{x}_m, t) + g(x_m, x_{m+1}, \dots, x_{m-1}), \quad (2)$$

$$m = 1, 2, \dots, N.$$

Here the periodic boundary condition imposes  $x_m(t) = x_{m+N}(t)$  for all  $m$ , the function  $f(x, \dot{x}, t)$  is given in Eq. (1), and  $g(x_1, \dots, x_N)$  is a coupling function, obeying the condition

$$g(x, \dots, x) = 0 \quad \text{for all } x. \quad (3)$$

The second-order differential equations (2) are reduced to a set of first-order differential equations,

$$\dot{x}_m = y_m, \quad (4a)$$

$$\dot{y}_m = f(x_m, y_m, t) + g(x_m, x_{m+1}, \dots, x_{m-1}), \quad (4b)$$

$$m = 1, 2, \dots, N.$$

Consider an initial orbit point  $\mathbf{z}(0) [= (z_1(0), \dots, z_N(0))]$ , where  $z_i = (x_i, y_i)$  ( $i = 1, \dots, N$ ). Then its Poincaré maps can be computed by sampling the orbit points  $\mathbf{z}(m)$  at the discrete time  $t = m$  ( $m = 1, 2, 3, \dots$ ). We will call the transformation  $\mathbf{z}(m) \rightarrow \mathbf{z}(m+1)$  the Poincaré map, and write  $\mathbf{z}(m+1) = P(\mathbf{z}(m))$ .

The  $2N$ -dimensional Poincaré map  $P$  has a cyclic permutation symmetry such that

$$\sigma^{-1} P \sigma(\mathbf{z}) = P(\mathbf{z}) \quad \text{for all } \mathbf{z}, \quad (5)$$

where  $\sigma$  is a cyclic permutation of  $\mathbf{z}$  such that  $\sigma(z_1, z_2, \dots, z_N) = (z_2, \dots, z_N, z_1)$  and  $\sigma^{-1}$  is its inverse. The set of all fixed points of  $\sigma$  forms a 2D synchronization plane, on which

$$x_1 = \dots = x_N, \quad y_1 = \dots = y_N. \quad (6)$$

It follows from Eq. (5) that the cyclic permutation  $\sigma$  commutes with the Poincaré map  $P$ , i.e.,  $\sigma P = P \sigma$ . Consequently, the 2D synchronization plane becomes invariant under  $P$ , i.e., if a point  $\mathbf{z}$  lies on the 2D synchronization plane, then its image  $P(\mathbf{z})$  also lies on it. An orbit is called a(n) (in-phase) synchronous orbit if it lies on the 2D invariant synchronization plane, i.e., it satisfies

$$x_1(t) = \dots = x_N(t) \equiv x^*(t), \quad y_1(t) = \dots = y_N(t) \equiv y^*(t). \quad (7)$$

Otherwise it is called an (out-of-phase) asynchronous orbit. Here we study only the synchronous orbits. They can be easily found from the uncoupled inverted pendulum (1), because the coupling function  $g$  satisfies the condition (3). Note also that for these synchronous orbits, the Poincaré map  $P$  also has the inversion symmetry such that

$$SPS(\mathbf{z}) = P(\mathbf{z}) \quad \text{for all } \mathbf{z}, \quad (8)$$

where  $S(\mathbf{z}) = -\mathbf{z}$ . If a synchronous orbit  $\{\mathbf{z}(t)\}$  of  $P$  is invariant under  $S$ , it is called a symmetric orbit. Otherwise, it is called an asymmetric orbit and has its ‘‘conjugate’’ orbit  $S\{\mathbf{z}(t)\}$ .

We now discuss the couplings between the inverted pendulums. Consider an element, say the  $m$ th element, in the  $N$  coupled inverted pendulums. Then the  $(m \pm \delta)$ th elements are called the  $\delta$ th neighbors of the  $m$ th element. Here we consider the case where the coupling extends to the  $K$ th ( $1 \leq K \leq (N/2)[(N-1)/2]$ ) for even (odd)  $N$  neighbor(s) with equal strength. Hereafter we will call the number  $K$  the range of the coupling interaction.

A general form of coupling for odd  $N$  ( $N \geq 3$ ) is given by

$$g(x_1, \dots, x_N) = \frac{c}{2K+1} \sum_{l=-K}^K [u(x_{1+l}) - u(x_1)]$$

$$= c \left[ \frac{1}{2K+1} \sum_{l=-K}^K u(x_{1+l}) - u(x_1) \right],$$

$$K = 1, \dots, \frac{N-1}{2}, \quad (9)$$

where  $c$  is a coupling parameter and  $u$  is a function of one variable. Note that the coupling extends to the  $K$ th neighbors with equal coupling strength, and the function  $g$  satisfies the condition (3). The extreme long-range interaction for  $K = (N-1)/2$  is called a global coupling, for which the coupling function  $g$  becomes

$$g(x_1, \dots, x_N) = \frac{c}{N} \sum_{m=1}^N [u(x_m) - u(x_1)]$$

$$= c \left[ \frac{1}{N} \sum_{m=1}^N u(x_m) - u(x_1) \right]. \quad (10)$$

This is a kind of mean-field coupling, in which each inverted pendulum is coupled to all the other ones with equal coupling strength. All the other couplings with  $K < (N-1)/2$  (e.g., nearest-neighbor coupling with  $K=1$ ) will be referred to as nonglobal couplings. The  $K=1$  case for  $N=3$  corresponds to both the global coupling and the nearest-neighbor coupling.

We next consider the case of even  $N$  ( $N \geq 2$ ). The form of coupling of Eq. (9) holds for the cases of nonglobal couplings with  $K=1, \dots, (N-2)/2$  ( $N \geq 4$ ). The global coupling for  $K=N/2$  ( $N \geq 2$ ) also has the form of Eq. (10), but it cannot have the form of Eq. (9), because there exists only one farthest neighbor for  $K=N/2$ , unlike the case of odd  $N$ .

The  $K=1$  case for  $N=2$  also corresponds to the nearest-neighbor coupling as well as to the global coupling, like the  $N=3$  case.

### III. STABILITY, BIFURCATIONS, AND LYAPUNOV EXPONENTS OF SYNCHRONOUS ORBITS

In this section we first discuss the stability of synchronous periodic orbits in the Poincaré map  $P$  of the coupled inverted pendulums, using the Floquet theory [15]. Bifurcations associated with the stability and Lyapunov exponents are then discussed.

The stability analysis of an orbit in many-coupled inverted pendulums can be conveniently carried out by Fourier transforming with respect to the discrete space  $\{m\}$  [16]. Consider an orbit  $\{x_m(t); m=1, \dots, N\}$  of the  $N$  coupled inverted pendulums (2). The discrete spatial Fourier transform of the orbit is

$$\mathcal{F}[x_m(t)] \equiv \frac{1}{N} \sum_{m=1}^N e^{-2\pi i m j / N} x_m(t) = \xi_j(t), \quad (11)$$

$$j=0, 1, \dots, N-1.$$

The Fourier transform  $\xi_j(t)$  satisfies  $\xi_j^*(t) = \xi_{N-j}(t)$  (\* denotes a complex conjugate), and the wavelength of a mode with index  $j$  is  $N/j$  for  $j \leq N/2$  and  $N/(N-j)$  for  $j > N/2$ . Here  $\xi_0$  corresponds to the synchronous (Fourier) mode of the orbit, while all the other  $\xi_j$ 's with nonzero indices  $j$  correspond to the asynchronous (Fourier) modes.

To determine the stability of a synchronous  $q$ -periodic orbit  $[x_1(t) = \dots = x_N(t) \equiv x^*(t) \text{ for all } t \text{ and } x^*(t) = x^*(t + q)]$ , we consider an infinitesimal perturbation  $\{\delta x_m(t)\}$  to the synchronous orbit, i.e.,  $x_m(t) = x^*(t) + \delta x_m(t)$  for  $m = 1, \dots, N$ . Linearizing the  $N$ -coupled inverted pendulums (2) at the synchronous orbit, we obtain

$$\delta \ddot{x}_m = \frac{\partial f(x^*, \dot{x}^*, t)}{\partial x^*} \delta x_m + \frac{\partial f(x^*, \dot{x}^*, t)}{\partial \dot{x}^*} \delta \dot{x}_m + \sum_{l=1}^N G_l(x^*) \delta x_{l+m-1}, \quad (12)$$

where

$$G_l(x) \equiv \left. \frac{\partial g(x_1, \dots, x_N)}{\partial x_l} \right|_{x_1 = \dots = x_N = x}. \quad (13)$$

Hereafter the functions  $G_l$ 's will be called "reduced" coupling functions of  $g(x_1, \dots, x_N)$ .

Let  $\delta \xi_j(t)$  be the Fourier transform of  $\delta x_m(t)$ , i.e.,

$$\delta \xi_j = \mathcal{F}[\delta x_m(t)] = \frac{1}{N} \sum_{m=1}^N e^{-2\pi i m j / N} \delta x_m, \quad (14)$$

$$j=0, 1, \dots, N-1.$$

Here  $\delta \xi_0$  is the synchronous-mode perturbation, and all the other  $\delta \xi_j$ 's with nonzero indices  $j$  are the asynchronous-mode perturbations. Then the Fourier transform of Eq. (12) becomes

$$\delta \ddot{\xi}_j = \frac{\partial f(x^*, \dot{x}^*, t)}{\partial \dot{x}^*} \delta \dot{\xi}_j + \left[ \frac{\partial f(x^*, \dot{x}^*, t)}{\partial x^*} + \sum_{l=1}^N G_l(x^*) e^{2\pi i (l-1)j/N} \right] \delta \xi_j, \quad (15)$$

$$j=0, 1, \dots, N-1.$$

Note that all the modes  $\delta \xi_j$ 's become decoupled for the synchronous orbit.

Equation (15) can also be put into the form

$$\begin{pmatrix} \delta \dot{\xi}_j \\ \delta \eta_j \end{pmatrix} = J_j(t) \begin{pmatrix} \delta \xi_j \\ \delta \eta_j \end{pmatrix}, \quad j=0, 1, \dots, N-1, \quad (16)$$

where

$$J_j(t) = \begin{pmatrix} 0 & 1 \\ \frac{\partial f(x^*, \dot{x}^*, t)}{\partial x^*} + \sum_{l=1}^N G_l(x^*) e^{2\pi i (l-1)j/N} & \frac{\partial f(x^*, \dot{x}^*, t)}{\partial \dot{x}^*} \end{pmatrix}. \quad (17)$$

Note that each  $J_j$  is a  $q$ -periodic matrix, i.e.,  $J_j(t) = J_j(t + q)$ . Using the Floquet theory [15], we study the stability of the synchronous  $q$ -periodic orbit against the  $j$ th-mode perturbation as follows. Let  $\Phi_j(t) = (\phi_j^{(1)}(t), \phi_j^{(2)}(t))$  be a fundamental solution matrix with  $\Phi_j(0) = I$ . Here  $\phi_j^{(1)}(t)$  and  $\phi_j^{(2)}(t)$  are two independent solutions expressed in column vector forms, and  $I$  is the  $2 \times 2$  unit matrix. Then a general solution of the  $q$ -periodic system has the following form:

$$\begin{pmatrix} \delta \xi_j(t) \\ \delta \eta_j(t) \end{pmatrix} = \Phi_j(t) \begin{pmatrix} \delta \xi_j(0) \\ \delta \eta_j(0) \end{pmatrix}, \quad (18)$$

$$j=0, 1, \dots, N-1,$$

Substitution of Eq. (18) into Eq. (16) leads to an initial-value problem to determine  $\Phi_j(t)$ :

$$\dot{\Phi}_j(t) = J_j(t)\Phi_j(t), \quad \Phi_j(0) = I. \quad (19)$$

Each  $2 \times 2$  matrix  $M_j \equiv \Phi_j(q)$ , which is obtained through integration of Eq. (19) over the period  $q$ , determines the stability of the  $q$ -periodic synchronous orbit against the  $j$ th-mode perturbation.

The characteristic equation of each matrix  $M_j$  ( $j = 0, 1, \dots, N-1$ ) is

$$\lambda_j^2 - \text{tr} M_j \lambda_j + \det M_j = 0, \quad (20)$$

where  $\text{tr} M_j$  and  $\det M_j$  denote the trace and determinant of  $M_j$ , respectively. The eigenvalues,  $\lambda_{j,1}$  and  $\lambda_{j,2}$  of  $M_j$  are called the Floquet (stability) multipliers, which characterize the stability of the synchronous  $q$ -periodic orbit against the  $j$ th-mode perturbation. Since the  $j=0$  case corresponds to the synchronous mode, the first pair of Floquet multipliers ( $\lambda_{0,1}, \lambda_{0,2}$ ) is called the pair of synchronous Floquet multipliers. On the other hand, all the other pairs of Floquet multipliers are called the pairs of asynchronous Floquet multipliers, because all the other cases of  $j \neq 0$  correspond to asynchronous modes.

As shown in Ref. [17],  $\det M_j$  is given by

$$\det M_j = e^{\int_0^q \text{tr} J_j dt} = e^{-2\pi\beta\Omega q}. \quad (21)$$

Note that all the matrices  $M_j$ 's have the same constant Jacobian determinant (less than unity). Accordingly, each pair of Floquet multipliers ( $\lambda_{j,1}, \lambda_{j,2}$ ) ( $j = 0, 1, \dots, N-1$ ) lies either on the circle of radius  $e^{-\frac{2\pi\beta\Omega q}{2}}$  or on the real axis in the complex plane. The synchronous periodic orbit is stable against the  $j$ th-mode perturbation when the pair of Floquet multipliers ( $\lambda_{j,1}, \lambda_{j,2}$ ) lies inside the unit circle in the complex plane. We first note that the Floquet multipliers never cross the unit circle in the complex plane, and hence Hopf bifurcations do not occur. Consequently, the synchronous periodic orbit can lose its stability against the  $j$ th-mode perturbation when a Floquet multiplier  $\lambda_j$  decreases (increases) through  $-1$  ( $1$ ) on the real axis.

A more convenient real quantity  $R_j$ , called the residue, and defined by

$$R_j \equiv \frac{1 + \det M_j - \text{tr} M_j}{2(1 + \det M_j)}, \quad j = 0, 1, \dots, N-1, \quad (22)$$

was introduced in Ref. [18] to characterize stability of periodic orbits in 2D dissipative maps with constant Jacobian determinants. Here the first one  $R_0$  is associated with the stability against the synchronous-mode perturbation, and hence it may be called the synchronous residue. On the other hand, all the other ones  $R_j$  ( $j \neq 0$ ) are called the asynchronous residues, because they are associated with the stability against the asynchronous-mode perturbations.

A synchronous periodic orbit is stable against the  $j$ th-mode perturbation when  $0 < R_j < 1$  [i.e., the pair of Floquet multipliers ( $\lambda_{j,1}, \lambda_{j,2}$ ) lies inside the unit circle in the complex plane]. When  $R_j$  decreases through 0 (i.e., a Floquet multiplier  $\lambda_j$  increases through 1), the synchronous periodic orbit loses its stability via saddle-node or pitchfork bifurcation (PFB). On the other hand, when  $R_j$  increases

through 1 (i.e., a Floquet multiplier  $\lambda_j$  decreases through  $-1$ ), it becomes unstable via period-doubling bifurcation (PDB). We also note that a(n) synchronous (asynchronous) bifurcation takes place for  $j=0$  ( $j \neq 0$ ). For each case of the synchronous (asynchronous) PFB and PDB, two types of supercritical and subcritical bifurcations occur. For the supercritical case of the synchronous (asynchronous) PFB and PDB, the synchronous periodic orbit loses its stability and gives rise to the birth of a pair of new stable synchronous (asynchronous) orbits with the same period and a new stable synchronous (asynchronous) period-doubled orbit, respectively. However, for the subcritical case of the synchronous (asynchronous) PFB and PDB, the synchronous periodic orbit becomes unstable by absorbing a pair of unstable synchronous (asynchronous) orbits with the same period and an unstable synchronous (asynchronous) period-doubled orbit, respectively. (For more details on bifurcations, refer to Ref. [19].)

It follows from condition (3) that the reduced coupling functions of Eq. (13) satisfy

$$\sum_{l=1}^N G_l(x) = 0. \quad (23)$$

Hence the matrix (17) for  $j=0$  becomes

$$J_0(t) = \begin{pmatrix} 0 & 1 \\ \frac{\partial f(x^*, \dot{x}^*, t)}{\partial x^*} & \frac{\partial f(x^*, \dot{x}^*, t)}{\partial \dot{x}^*} \end{pmatrix}. \quad (24)$$

This is just the linearized Jacobian matrix for the case of the uncoupled inverted pendulum [11]. Hence the synchronous residue  $R_0$  becomes the same as the residue of the uncoupled inverted pendulum, i.e., it depends only on the amplitude  $A$ . While there is no coupling effect on  $R_0$ , the coupling affects all the other asynchronous residues  $R_j$  ( $j \neq 0$ ).

In case of the global coupling of Eq. (10), the reduced coupling functions become

$$G_l(x) = \begin{cases} (1-N)G(x) & \text{for } l=1 \\ G(x) & \text{for } l \neq 1, \end{cases} \quad (25)$$

where  $G(x) = (c/N)u'(x)$ . Substituting  $G_l$ 's into the second term of the (2,1) entry of the matrix  $J_j(t)$  of Eq. (17), we have

$$\sum_{l=1}^N G_l(x) e^{2\pi i(l-1)j/N} = \begin{cases} 0 & \text{for } j=0 \\ -c u'(x) & \text{for } j \neq 0. \end{cases} \quad (26)$$

Hence all the asynchronous residues  $R_j$  ( $j \neq 0$ ) become the same, i.e.,  $R_1 = \dots = R_{N-1}$ . Consequently, there exist only two independent residues  $R_0$  and  $R_1$ , independently of  $N$ .

We next consider the nonglobal coupling of form (9), and define

$$G(x) \equiv \frac{c}{2K+1} u'(x), \quad (27)$$

where  $1 \leq K \leq (N-2)/2[(N-3)/2]$  for even (odd)  $N$  larger than 3. Then we have

$$G_l(x) = \begin{cases} -2KG(x) & \text{for } l=1 \\ G(x) & \text{for } 2 \leq l \leq 1+K \text{ or for } N+1-K \leq l \leq N \\ 0 & \text{otherwise.} \end{cases} \quad (28)$$

Substituting the reduced coupling functions into the matrix  $J_j(t)$ , the second term of the (2,1) entry of  $J_j(t)$  becomes

$$\sum_{l=1}^N G_l(x) e^{2\pi i(l-1)j/N} = -S_N(K,j) c u'(x), \quad (29)$$

where

$$S_N(K,j) \equiv \frac{4}{2K+1} \sum_{k=1}^K \sin^2 \frac{\pi j k}{N} = 1 - \frac{\sin(2K+1) \frac{\pi j}{N}}{(2K+1) \sin \frac{\pi j}{N}}. \quad (30)$$

Hence, unlike the global-coupling case, all the asynchronous residues vary depending on the coupling range  $K$  as well as on the mode number  $j$ . Since  $S_N(K,j) = S_N(K,N-j)$ , the residues satisfy

$$R_j = R_{N-j}, \quad j = 0, 1, \dots, N-1. \quad (31)$$

Thus it is sufficient to consider only the case of  $0 \leq j \leq (N/2) [(N-1)/2]$  for even (odd)  $N$ . Comparing the expression in Eq. (29) with that in Eq. (26) for  $j \neq 0$ , one can easily see that they are the same except for the factor  $S_N(K,j)$ . Consequently, making a change of the coupling parameter  $c \rightarrow c/[S_N(K,j)]$ , the residue  $R_j$  for the nonglobal coupling case of range  $K$  becomes the same as that for the global-coupling case.

When the synchronous residue  $R_0$  of a synchronous periodic orbit increases through 1, the synchronous periodic orbit loses its stability via synchronous supercritical PDB, giving rise to the birth of a new synchronous period-doubled orbit. Here we are interested in such synchronous supercritical PDB's. Thus, for each mode with nonzero index  $j$  we consider a region in the  $A$ - $c$  plane in which the synchronous periodic orbit is stable against the perturbations of both modes with indices 0 and  $j$ . This stable region is bounded by four bifurcation curves determined by the equations  $R_0=0$  and 1 and  $R_j=0$  and 1, and it will be denoted by  $U_N$ .

For the case of global coupling, those stable regions coincide, irrespectively of  $N$  and  $j$ , because all the asynchronous residues  $R_j$ 's ( $j \neq 0$ ) are the same, independently of  $N$ . The stable region for this global-coupling case will be denoted by  $U_G$ . Note that  $U_G$  itself is just the stability region of the synchronous periodic orbit, irrespectively of  $N$ , because the synchronous periodic orbit is stable against the perturbations of all synchronous and asynchronous modes in the region  $U_G$ . Thus the stability diagram of synchronous orbits of period  $2^n$  ( $n=0,1,2,\dots$ ) in the  $A$ - $c$  plane becomes the same, independently of  $N$ .

However, the stable region  $U_N$  varies depending on the coupling range  $K$  and the mode number  $j$  for the nonglobal-

coupling cases, i.e.,  $U_N = U_N(K,j)$ . To find the stability region of a synchronous periodic orbit in the  $N$  coupled inverted pendulums with a given  $K$ , one may start with the stability region  $U_G$  for the global-coupling case. Rescaling the coupling parameter  $c$  by a scaling factor  $1/S_N(K,j)$  for each nonzero  $j$ , the stable region  $U_G$  is transformed into a stable region  $U_N(K,j)$ . Then the stability region of the synchronous periodic orbit is given by the intersection of all such stable regions  $U_N$ 's.

Finally, we briefly discuss Lyapunov exponents of a synchronous orbit in the Poincaré map  $P$ , characterizing the mean exponential rate of divergence of nearby orbits [20]. As shown in Eq. (15), all the synchronous and asynchronous modes of a perturbation to a synchronous orbit becomes decoupled. Hence each matrix  $M_j [\equiv \Phi_j(1)]$  with  $q=1$  determines the pair of Lyapunov exponents  $(\sigma_{j,1}, \sigma_{j,2})$  ( $j=0,1,\dots,N-1$ ), characterizing the average exponential rates of divergence of the  $j$ th mode perturbation, where  $\sigma_{j,1} \geq \sigma_{j,2}$ . Since each  $M_j$  has the same constant Jacobian determinant (i.e.,  $\det M_j = e^{-2\pi\beta\Omega}$ ), each pair of Lyapunov exponents satisfies  $\sigma_{j,1} + \sigma_{j,2} = -2\pi\beta\Omega$ . Note also that the first pair of synchronous Lyapunov exponents  $(\sigma_{0,1}, \sigma_{0,2})$  is just the pair of the Lyapunov exponents of the uncoupled inverted pendulum [11], and the coupling affects only all the other pairs of asynchronous Lyapunov exponents  $(\sigma_{j,1}, \sigma_{j,2})$  ( $j \neq 0$ ). Furthermore, all the pairs of the asynchronous Lyapunov exponents for the global-coupling case become the same [i.e.,  $(\sigma_{1,1}, \sigma_{1,2}) = \dots = (\sigma_{N-1,1}, \sigma_{N-1,2})$ ], as in the case of the asynchronous residues.

#### IV. CRITICAL SCALING BEHAVIORS OF PERIOD DOUBLINGS

In this section, by varying the two parameters  $A$  and  $c$ , we study the critical scaling behaviors of synchronous PDB's in the  $N$  symmetrically coupled inverted pendulums for  $\beta = 0.2$  and  $\Omega = 0.1$ . It is found that the critical behaviors depend on the coupling range. In the global-coupling case, in which each inverted pendulum is coupled to all the other ones with equal coupling strength, the zero-coupling critical point and an infinity of critical line segments constitute the same critical set, independently of  $N$ . However, for any other nonglobal-coupling cases, the structure of the critical set becomes different from that for the global-coupling case, because of a significant change in the stability diagram of the synchronous  $2^n$ -periodic orbits ( $n=0,1,2,\dots$ ). The critical scaling behaviors on the critical set are found to be the same as those for the abstract system of the coupled 1D maps [14]. We thus consider separately two kinds of couplings, the global- and nonglobal-coupling cases.

##### A. Global coupling

We first study the  $N$  globally coupled inverted pendulums with the coupling function of form (10). As shown in Sec.

III, a synchronous periodic orbit is stable when all its residues  $R_j$  ( $j=0,1,\dots,N-1$ ) defined in Eq. (22) lie between 0 and 1 (i.e.,  $0 < R_j < 1$ ). Here  $R_0$  is the synchronous residue determining the stability against the synchronous-mode perturbation, while all the other ones  $R_j$  ( $j \neq 0$ ) are the asynchronous residues determining the stability against the asynchronous-mode perturbations. For the globally coupled case, all the asynchronous residues become the same, independently of  $j$ , and hence only one independent asynchronous residue (e.g.,  $R_1$ ) exists. Accordingly, the stability region of a synchronous periodic orbit becomes bounded by four bifurcation lines determined by the equations  $R_0=0$  and 1 and  $R_1=0$  and 1. Here the  $R_0=0$  and 1 ( $R_1=0$  and 1) lines correspond to the synchronous (asynchronous) PFB and PDB lines, respectively. In such a way, we obtain the stability diagram of the synchronous  $2^n$ -periodic orbits ( $n=0,1,2,\dots$ ) in the  $A$ - $c$  plane. Note also that the stability diagram becomes the same, independently of  $N$ , because all the asynchronous residues  $R_j$  ( $j \neq 0$ ) for each synchronous orbit are also the same, irrespective of  $N$ . Consequently, the structure of the critical set and the critical behaviors for the global-coupling case become the same, independently of  $N$ .

As an example, we consider a linearly coupled case in which the coupling function (10) is

$$g(x_1, \dots, x_N) = c \left[ \frac{1}{N} \sum_{m=1}^N x_m - x_1 \right]. \quad (32)$$

As in the uncoupled inverted pendulum [11], the coupled inverted pendulums exhibit multiple period-doubling transitions to chaos. Here we study the first three period-doubling transitions to chaos. For each period-doubling transition to chaos, the zero-coupling critical point and an infinity of critical line segments constitute the critical set in the  $A$ - $c$  plane. Three kinds of critical behaviors associated with the scaling of the coupling parameter  $c$  are found on the critical set, while the critical scaling behavior of the amplitude  $A$  is always the same as that of the uncoupled inverted pendulum. Note that the structure of the critical set and the critical behaviors for the coupled inverted pendulums are found to be the same as those for the coupled 1D maps [14].

Figure 1(a) shows the stability diagram of the synchronous orbits with low period  $q=1$  and 2. The stable region of a synchronous orbit is bounded by its PDB and PFB lines. The horizontal (nonhorizontal) solid and dashed boundary lines correspond to synchronous (asynchronous) PDB and PFB lines, respectively. Each bifurcation may be supercritical or subcritical.

We first consider the bifurcations associated with stability of the synchronous inverted stationary point, corresponding to the vertically up configuration [i.e.,  $x_1(t) = \dots = x_N(t) \equiv x^*(t) = \frac{1}{2}$  and  $y_1(t) = \dots = y_N(t) \equiv y^*(t) = 0$ ]. The inverted state is a symmetric one with respect to the inversion symmetry  $S$ . Its stability region is denoted by the IS in Fig. 1(a). For the unforced case of  $A=0$ , the inverted state is obviously unstable. However, when crossing the horizontal dashed boundary line of the IS, its first resurrection occurs, i.e., it becomes stabilized with birth of a pair of unstable synchronous asymmetric orbits with period 1 via a subcritical PFB. (For more details on the resurrection of the inverted state, refer to Ref. [11].) This stabilized inverted state desta-

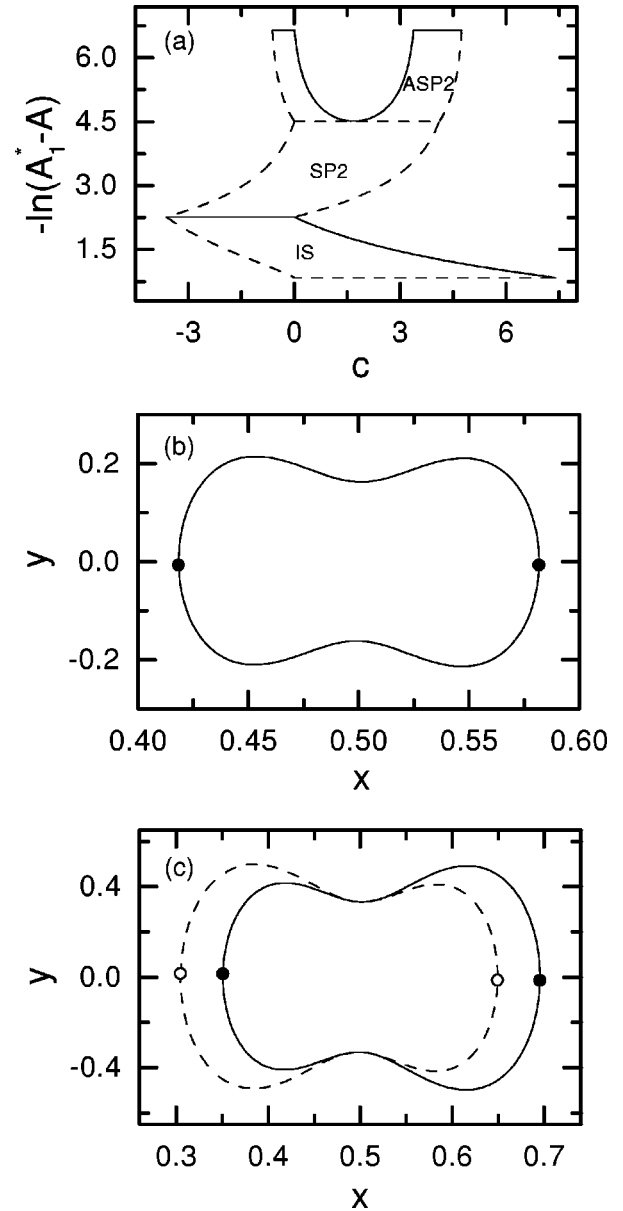


FIG. 1. (a) Stability diagram of the synchronous orbits of low period  $q=1$  and 2 in  $N$  linearly coupled inverted pendulums with global coupling. Here  $A_1^*$  ( $=0.575154\dots$ ) is just the first period-doubling transition point of the uncoupled inverted pendulum. The stable regions of the inverted stationary point, a symmetric 2-periodic orbit, and an asymmetric 2-periodic orbit are denoted by SP, SP2, and ASP2, respectively. The horizontal (nonhorizontal) solid and dashed boundary lines correspond to synchronous (asynchronous) PDB and PFB lines, respectively. (b) Phase portraits for  $A=0.5$ . The phase flow of a symmetric 2-periodic orbit born via a synchronous supercritical PDB is denoted by a solid curve, and its Poincaré maps are represented by the solid circles. (c) Phase portraits for  $A=0.57$ . The phase flows of a conjugate pair of asymmetric 2-periodic orbits born via synchronous supercritical PFB are shown: one is denoted by a solid curve, while the other one is denoted by a dashed curve. Their Poincaré maps are also represented by solid and open circles, respectively.

bilizes again through asynchronous PDB and PFB when the nonhorizontal solid and dashed boundary curves are crossed, respectively. However, it becomes unstable via a synchronous supercritical PDB when crossing the horizontal solid

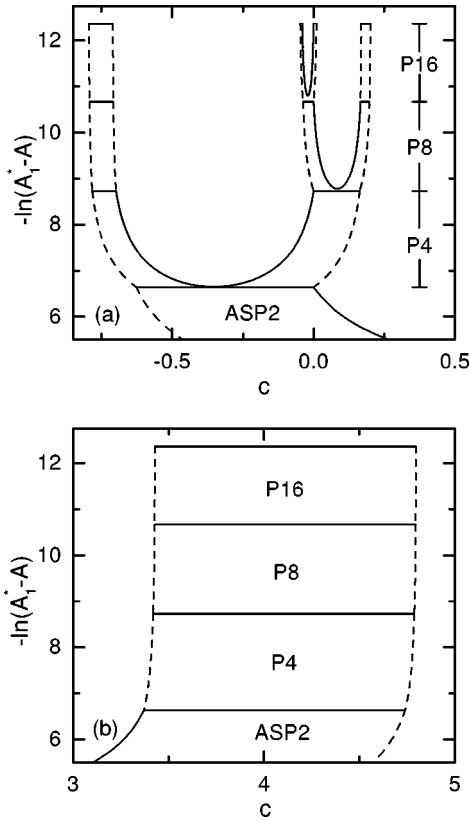


FIG. 2. Stability diagram of synchronous asymmetric  $2^n$ -periodic ( $n = 1, 2, 3$ , and  $4$ ) orbits of level  $n$  born via synchronous supercritical PDB's. PN denotes the stable region of an asymmetric orbit of period  $N$  ( $N = 2, 4, 8$ , and  $16$ ). The solid and dashed boundary lines represent the same as those in Fig. 1. The stability diagram starting from the left (right) side of the ASP2 is shown in (a) [(b)]. Note its treelike structure.

boundary line, and gives rise to the birth of a new synchronous orbit of period 2. This new synchronous 2-periodic orbit also is a symmetric one with respect to the inversion symmetry  $S$ , as shown in Fig. 1(b) and its stable region is denoted by the SP2 in Fig. 1(a). This synchronous symmetric orbit of period 2 loses its stability through asynchronous PFB's when crossing the nonhorizontal dashed boundary curves. However, it becomes unstable via a synchronous supercritical PFB when the horizontal dashed boundary line is crossed, and consequently a pair of new stable synchronous orbits with the same period 2 appears. Note that the new pair of synchronous orbits is a conjugate pair of asymmetric orbits with respect to the inversion symmetry  $S$ , which is shown in Fig. 1(c). That is, the inversion symmetry is broken due to the symmetry-breaking PFB. The stable region of the asymmetric orbits of period 2 is denoted by the ASP2 in Fig. 1(a). Each synchronous asymmetric 2-periodic orbit becomes unstable via a synchronous supercritical PDB when the horizontal solid boundary line is crossed, and gives rise to the birth of a new synchronous asymmetric 4-periodic orbit. Here we are interested in such synchronous supercritical PDB's.

Figure 2 shows the stability diagram of synchronous asymmetric orbits born by synchronous supercritical PDB's. Each synchronous asymmetric orbit of level  $n$  (period  $2^n$ ,  $n = 1, 2, 3, \dots$ ) loses its stability at the horizontal solid bound-

ary line of its stable region via a synchronous supercritical PDB, and gives rise to the birth of a synchronous asymmetric period-doubled orbit of level  $n + 1$ . Such an infinite sequence ends at a finite value of  $A_1^* = 0.575154\dots$ , which is just the first period-doubling transition point of the uncoupled inverted pendulum [11]. Consequently, a synchronous quasi-periodic orbit, whose maximum synchronous Lyapunov exponent is zero (i.e.,  $\sigma_{0,1} = 0$ ), exists on the  $A = A_1^*$  line.

We examine the treelike structure of the stability diagram in Fig. 2, which consists of an infinite pile of  $U$ -shaped and rectangular-shaped regions. Note that the treelike structure is asymptotically the same as that in the coupled 1D maps [14]. The  $U$ -shaped branching is repeated at one side of each  $U$ -shaped region, including the  $c = 0$  line segment. The branching side will be referred to as the zero  $c$  side. However, the other side of each  $U$ -shaped region grows like a chimney without any further branchings [as an example, see the branch in Fig. 2(b) starting from the right side of the  $U$ -shaped region of the ASP2]. As in the coupled 1D maps [14], this rule governs the asymptotic behavior of the treelike structure.

A sequence of connected stability regions with increasing period is called a ‘‘period-doubling route’’ [14]. There are two kinds of period-doubling routes. The sequence of the  $U$ -shaped regions with the zero  $c$  sides converges to the zero-coupling point  $c = 0$  on the  $A = A_1^*$  line. It will be referred to as the  $U$  route. On the other hand, a sequence of rectangular regions in each chimney converges to a critical line segment on the  $A = A_1^*$  line. For example, the sequence of the rectangular regions in Fig. 2(b) converges to a critical line segment joining the left end point  $c_l (= 3.427742\dots)$  and the right end point  $c_r (= 4.796277\dots)$  on the  $A = A_1^*$  line. This kind of route will be called a  $C$  route. Note that there are infinitely many  $C$  routes, while the  $U$  route converging to the zero-coupling critical point  $(A_1^*, 0)$  is unique. Hence, an infinite number of critical line segments, together with the zero-coupling critical point, constitute the critical set.

We now study the critical behaviors on the critical set. First, consider the case of the  $U$  route ending at the zero-coupling critical point. We follow the synchronous orbits of period  $q = 2^n$  up to level  $n = 8$  in the  $U$  route, and obtain a self-similar sequence of parameters  $(A_n, c_n)$ , at which each orbit of level  $n$  has some given synchronous and asynchronous residues  $R_0$  and  $R_1 (= R_2 = \dots = R_{N-1})$  (e.g.,  $R_0 = 1$  and  $R_1 = 0$ ). Then the sequence  $\{(A_n, c_n)\}$  converges geometrically to the zero-coupling critical point  $(A_1^*, 0)$ . As in the uncoupled inverted pendulum [11], the sequence  $\{A_n\}$  obeys a scaling law

$$\Delta A_n \sim \delta^{-n} \quad \text{for large } n, \tag{33}$$

where  $\Delta A_n = A_n - A_{n-1}$  and  $\delta \approx 4.67$ . The value of the scaling factor  $\delta$  agrees well with the Feigenbaum constant ( $= 4.669\dots$ ) of the 1D map [12]. We also note that the sequence  $\{c_n\}$  obeys a scaling law

$$\Delta c_n \sim \mu^{-n} \quad \text{for large } n, \tag{34}$$

where  $\Delta c_n = c_n - c_{n-1}$ . The sequence of the scaling factor  $\{\mu_n\}$  ( $= \Delta c_n / \Delta c_{n+1}$ ) of level  $n$  is listed in the second column of Table I, and converges to a constant  $\mu$  ( $\approx -2.5$ ),

TABLE I. For the case of the  $U$  route, the scaling factors  $\mu_n$  and  $\nu_n$  in the scaling for the coupling parameter and the slope of the asynchronous residue at the zero-coupling critical point are shown in the second and third columns, respectively.

$n$	$\mu_n$	$\nu_n$
4	-3.517	-2.958
5	-2.904	-2.627
6	-2.530	-2.480
7	-2.495	-2.522

which agrees well with the coupling-parameter scaling factor  $\alpha$  ( $\approx -2.502 \dots$ ) of the coupled 1D maps near the zero-coupling critical point [14]. It was also shown in Ref. [14] that the scaling factor  $\alpha$  is just the largest relevant ‘‘coupling eigenvalue’’ (CE) of the zero-coupling fixed map of the renormalization transformation for the case of the coupled 1D maps.

We also study the coupling effect on the asynchronous residue  $R_{1,n}$  of the synchronous orbit of period  $2^n$  near the zero-coupling critical point  $(A_1^*, 0)$ . Figure 3 shows three plots of  $R_{1,n}(A_1^*, c)$  versus  $c$  for  $n=5, 6$  and  $7$ . For  $c=0$ ,  $R_{1,n}$  converges to a constant  $R_1^*$  ( $\approx 1.30059 \dots$ ), called the critical asynchronous residue, as  $n \rightarrow \infty$ . However, when  $c$  is nonzero  $R_{1,n}$  diverges as  $n \rightarrow \infty$ , i.e., its slope  $S_n$  ( $\equiv \partial R_{1,n} / \partial c|_{(A_1^*, 0)}$ ) at the zero-coupling critical point diverges as  $n \rightarrow \infty$ .

As in the scaling for the coupling parameter  $c$ , the sequence  $\{S_n\}$  also obeys a scaling law

$$S_n \sim \nu^n \quad \text{for large } n. \quad (35)$$

The scaling factor  $\nu_n$  ( $= S_{n+1} / S_n$ ) of level  $n$  is listed in the third column of Table I, and converges to a constant  $\nu$  ( $\approx -2.5$ ) as  $n \rightarrow \infty$ . Note also that the value of  $\nu$  agrees well with that of the largest relevant CE  $\alpha$  of the zero-coupling fixed map.

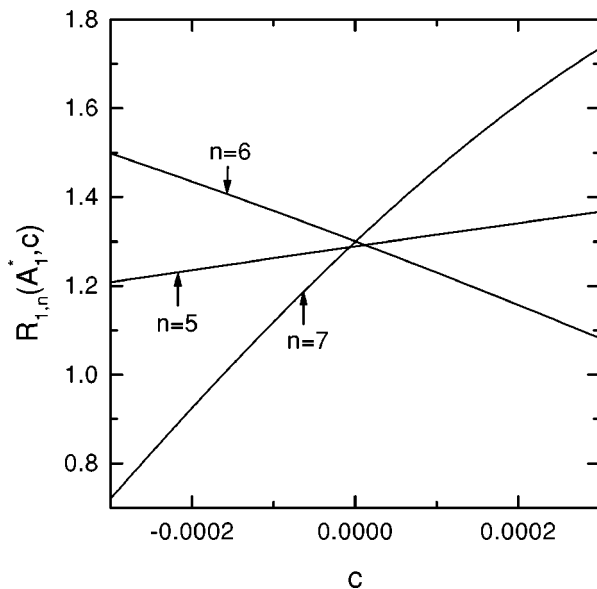


FIG. 3. Plots of the asynchronous residue  $R_{1,n}(A_1^*, c)$  vs  $c$  near the zero-coupling critical point for  $n=5, 6$ , and  $7$ .

We next consider the cases of  $C$  routes, each of which converges to a critical line segment. Two kinds of additional critical behaviors are found at each critical line segment; one critical behavior exists at both ends, and the other critical behavior exists at interior points. In each  $C$  route, there are two kinds of self-similar sequences of parameters  $(A_n, c_n)$ , at which each synchronous orbit of level  $n$  has some given synchronous and asynchronous residues  $R_0$  and  $R_1$ ; the one converges to the left end point of the critical line segment and the other converges to the right end point. As an example, consider the  $C$  route in Fig. 2(b), which converges to the critical line segment with two ends  $(A_1^*, c_l)$  and  $(A_1^*, c_r)$ . We follow, in the  $C$  route, two self-similar sequences of parameters, one converging to the left end and the other converging to the right end. In both cases, the sequence  $\{A_n\}$  converges geometrically to its accumulation value  $A_1^*$  with the 1D scaling factor  $\delta$  ( $\approx 4.67$ ) like the case of the  $U$  route. The sequences  $\{c_n\}$  for both cases also obey the scaling law

$$\Delta c_n \sim \mu^{-n} \quad \text{for large } n, \quad (36)$$

where  $\Delta c_n = c_n - c_{n-1}$ . The sequence of the scaling factor  $\mu_n$  ( $= \Delta c_n / \Delta c_{n+1}$ ) of level  $n$  is listed in Table II, and converges to its limit value  $\mu$  ( $\approx 2$ ). We also note that the value of  $\mu$  agrees well with that of the coupling-parameter scaling factor ( $\nu=2$ ) of the coupled 1D maps near both ends of each critical line segment [14]. It was also shown in Ref. [14] that the scaling factor  $\nu$  ( $=2$ ) is just the only relevant CE of a nonzero-coupling fixed map of the renormalization transformation for the case of the coupled 1D maps.

Figure 4(a) shows the behavior of the asynchronous residue  $R_{1,n}(A_1^*, c)$  of the synchronous orbit of period  $2^n$  ( $n=5, 6$  and  $7$ ) near the critical line segment in Fig. 2(b). Magnified views near both ends  $c_l$  and  $c_r$  are also given in Figs. 4(b) and 4(c), respectively. For  $c=c_l$  and  $c_r$ ,  $R_{1,n}$  converges to a critical asynchronous residue  $R_1^*$  ( $=0$ ) as  $n \rightarrow \infty$ , which is different from that for the zero-coupling case. The sequence of the slope  $S_n$  of  $R_{1,n}$  at both ends obeys well the scaling law

$$S_n \sim \nu^n \quad \text{for large } n. \quad (37)$$

The two sequences of the scaling factors  $\nu_n$  ( $= S_{n+1} / S_n$ ) of level  $n$  at both ends are listed in Table III, and converge to their limit values  $\nu \approx 2$ , which agrees well with the only CE ( $\nu=2$ ) of the nonzero-coupling fixed map governing the

TABLE II. We followed, in the  $C$  route in Fig. 2(b), two self-similar sequences of parameters  $(A_n, c_n)$ , at which the pair of residues  $(R_{0,n}, R_{1,n})$  of the synchronous orbit with period  $2^n$  is  $(1, 0.1)$ . They converge to both ends of the critical line segment. The scaling factors of the coupling parameter at the left and right ends are shown in the second and third columns, respectively. In both cases the scaling factors seem to converge to the same limit value  $\mu \approx 2$ .

$n$	$\mu_n$	$\mu_n$
4	3.66	3.93
5	2.81	3.04
6	2.02	2.15
7	1.93	1.99

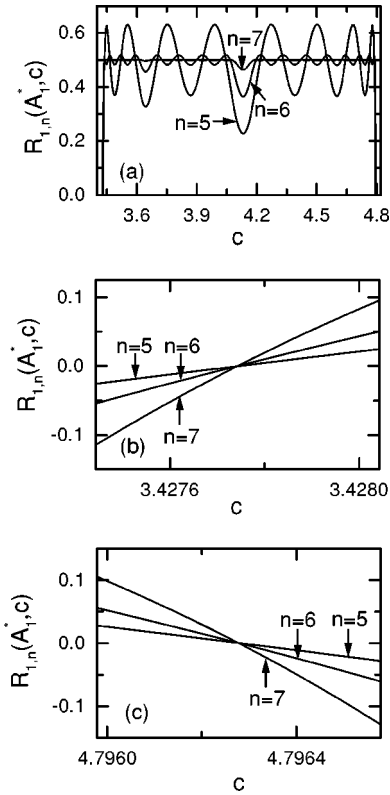


FIG. 4. (a) Plots of the asynchronous residue  $R_{1,n}(A_1^*, c)$  vs  $c$  near the critical line in Fig. 2(b) for  $n=5, 6$ , and  $7$ . Their magnified views near the both ends  $c_l$  and  $c_r$  are also given in (b) and (c), respectively.

critical behavior at both ends for the case of the coupled 1D maps. However, for any fixed value of  $c$  inside the critical line segment,  $R_{1,n}$  converges to a critical asynchronous residue  $R_1^*$  ( $=0.5$ ) as  $n \rightarrow \infty$  [see Fig. 4(a)]. This case of  $R_1^* = 0.5$  corresponds to the superstable case of  $\lambda_1^* = 0$  ( $\lambda_1^*$ : the critical asynchronous Floquet multiplier) for the coupled 1D maps [14], because Eq. (22) of  $R$  for the case of 2D maps reduces to the equation of  $R = 0.5 \times (1 - \lambda)$  for the case of 1D maps. We also note that as in the case of the coupled 1D maps, there exists no scaling factor of the coupling parameter inside the critical line segment, and hence the coupling parameter becomes an irrelevant one at interior critical points. Thus the critical behavior inside the critical line segment becomes the same as that of the uncoupled inverted pendulum (i.e., that of the 1D map), which will be discussed in more details below. This kind of 1D-like critical behavior

TABLE III. The scaling factors  $\nu_n$ 's in the scaling for the slope of the asynchronous residue at the left and right ends of the critical line segment in Fig. 2(b) are shown in the second and third columns, respectively.

$n$	$\nu_n$	$\nu_n$
4	2.528	2.525
5	2.071	2.072
6	2.001	2.001
7	2.000	2.000

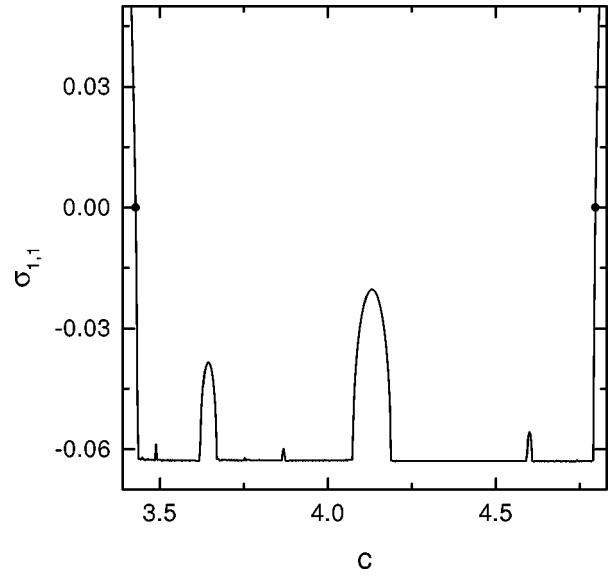


FIG. 5. Plot of the maximum asynchronous Lyapunov exponent  $\sigma_{1,1}$  of the synchronous quasiperiodic orbit near the critical line in Fig. 2(b). This plot consists of 450  $c$  values, each of which is obtained by iterating the Poincaré map  $P$  20 000 times to eliminate transients and then averaging over another 5000 iterations. The values of  $\sigma_{1,1}$  at both ends of the critical line are zero, which are denoted by solid circles.

was found to be governed by another nonzero-coupling fixed map with no relevant CE for the case of the coupled 1D maps [14].

There exists a synchronous quasiperiodic orbit on the  $A = A_1^*$  line. As mentioned in Sec. III, its synchronous Lyapunov exponents are the same as the Lyapunov exponents of the uncoupled inverted pendulum, i.e.,  $\sigma_{0,1} = 0$  and  $\sigma_{0,2} = -2\pi\beta\Omega$ . The coupling affects only the pair of asynchronous Lyapunov exponents  $(\sigma_{1,1}, \sigma_{1,2})$  [ $= (\sigma_{2,1}, \sigma_{2,2}) = \dots = (\sigma_{N-1,1}, \sigma_{N-1,2})$ ]. The maximum asynchronous Lyapunov exponent  $\sigma_{1,1}$  near the critical line segment in Fig. 2(b) is shown in Fig. 5. Inside the critical line segment ( $c_l < c < c_r$ ), the synchronous quasiperiodic orbit on the synchronization plane becomes a synchronous attractor with  $\sigma_{1,1} < 0$ . Since the dynamics on the synchronous attractor is the same as that of the uncoupled inverted pendulum, the critical maps at interior points exhibit essentially 1D-like critical behaviors, because the critical behavior of the uncoupled inverted pendulum is the same as that of the 1D maps [11]. However, as the coupling parameter  $c$  passes through  $c_l$  and  $c_r$ , the maximum asynchronous Lyapunov exponent  $\sigma_{1,1}$  of the synchronous quasiperiodic orbit increases from zero. Consequently, the synchronous quasiperiodic orbit ceases to be an attractor outside the critical line segment, and the system of the coupled inverted pendulums is asymptotically attracted to another synchronous rotational attractor of period 1.

What happens beyond the first period-doubling transition point  $A_1^*$  is also interesting. As in the uncoupled 1D inverted pendulum [11], with increasing the amplitude  $A$  further from  $A = A_1^*$ , the unstable inverted state undergoes a cascade of resurrections, i.e., it will restabilize after it loses its stability, destabilize again, and so forth *ad infinitum*. For each case of the resurrections, an infinite sequence of PDB's leading to

chaos follows. Consequently, the coupled inverted pendulums exhibit multiple period-doubling transitions to chaos.

As the first example, we consider the second period-doubling transition to chaos. Figure 6(a) shows the second stability diagram of the synchronous inverted stationary point and asymmetric orbits of level  $n$  (period  $2^n$ ,  $n=0,1,2$ , and 3) in the  $A$ - $c$  plane. When crossing the horizontal solid boundary line of its stability region IS, the unstable inverted state restabilizes with birth of a new unstable synchronous symmetric orbit of period 2 via a synchronous subcritical PDB. This is the second resurrection of the inverted state. However, when the horizontal dashed boundary line is crossed, the stabilized inverted state becomes unstable via a synchronous supercritical PFB, which results in the birth of a conjugate pair of synchronous asymmetric orbits with period 1. Then each synchronous asymmetric orbit of level  $n$  becomes unstable at the horizontal solid boundary line of its stability region via a synchronous supercritical PDB, and gives rise to the birth of a synchronous asymmetric period-doubled orbit of level  $n+1$ . Such an infinite sequence terminates at a finite value of  $A_2^*$  ( $=3.829784\dots$ ), which is the second period-doubling transition point of the uncoupled inverted pendulum [11]. Note that the treelike structure of the stability diagram in Fig. 6(a) is essentially the same as that in Fig. 2(a). Hence, the critical set also consists of the zero-coupling critical point and an infinite number of critical line segments, as in the first period-doubling transition case. In order to study the critical behaviors on the critical set, we follow the synchronous asymmetric orbits up to level  $n=7$  in the  $U$  route and in the rightmost  $C$  route. It is found that the critical behaviors are the same as those for the first period-doubling transition case. That is, there exist three kinds of critical behaviors at the zero-coupling critical point, both ends of each critical line segment and interior points.

As the second example, we also consider the third period-doubling transition to chaos. The third stability diagram of the synchronous orbits with  $q=1, 2, 4$ , and 8 is shown in Fig. 6(b). A synchronous subcritical PFB occurs when crossing the horizontal dashed boundary line of the IS. Consequently, the unstable inverted state restabilizes with birth of a pair of unstable orbits with period 1. This is the third resurrection of the inverted state. However, the stabilized inverted state becomes unstable via a synchronous supercritical PDB when the horizontal solid boundary line of the IS is crossed, and gives rise to the birth of a symmetric 2-periodic orbit. The subsequent bifurcation behaviors are the same as those for the first period-doubling transition to chaos. That is, a third infinite sequence of synchronous supercritical PDB's follows and ends at a finite value  $A_3^*$  ( $=10.675090\dots$ ), which is the third period-doubling transition point of the uncoupled inverted pendulum [11]. Note also that the treelike structure of the third stability diagram is essentially the same as that in Fig. 2(a). Hence the critical set is composed of the zero-coupling critical point and an infinity of critical line segments. Furthermore, the critical behaviors on the critical set are found to be the same as those for the first period-doubling transition case.

In addition to the linear-coupling case (32), we have also studied two other nonlinear-coupling cases:

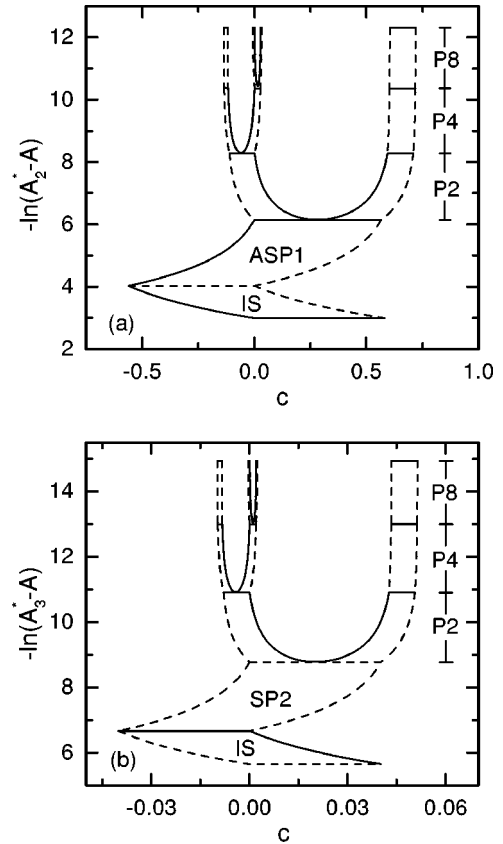


FIG. 6. (a) Second and (b) third stability diagrams of synchronous periodic orbits. Here  $A_2^*$  ( $=3.829784\dots$ ) and  $A_3^*$  ( $=10.675090$ ) are just the second and third period-doubling transition points of the uncoupled inverted pendulum, respectively. The stable regions of the inverted stationary point, an asymmetric orbit of period 1, a symmetric 2-periodic orbit, and an asymmetric  $N$ -periodic ( $N=2, 4$ , and 8) orbit are denoted by IS, ASP1, SP2, and PN, respectively. The solid and dashed boundary lines also represent the same as those in Fig. 1.

$$g(x_1, \dots, x_N) = c \left[ \frac{1}{N} \sum_{m=1}^N x_m^n - x_1^n \right], \quad n=2 \text{ and } 3. \quad (38)$$

First stability diagrams of the synchronous orbits for the cases of the quadratic and cubic couplings are shown in Figs. 7(a) and 7(b), respectively. Their treelike structures are essentially the same as that in Fig. 2(a). Hence, the zero-coupling critical point and an infinite number of critical line segments constitute the critical set for each nonlinear-coupling case. Moreover, the critical behaviors for these nonlinear-coupling cases are also found to be the same as those for the linear-coupling case.

### B. Nonglobal coupling

Here we study the nonglobal-coupling cases with the coupling range  $K < (N/2)[(N-1)/2]$  for even (odd)  $N$ . The structure of the critical set becomes different from that for the global-coupling case, because of a significant change in the stability diagram of the synchronous orbits with period  $2^n$  ( $n=0,1,2,\dots$ ), as will be seen below.

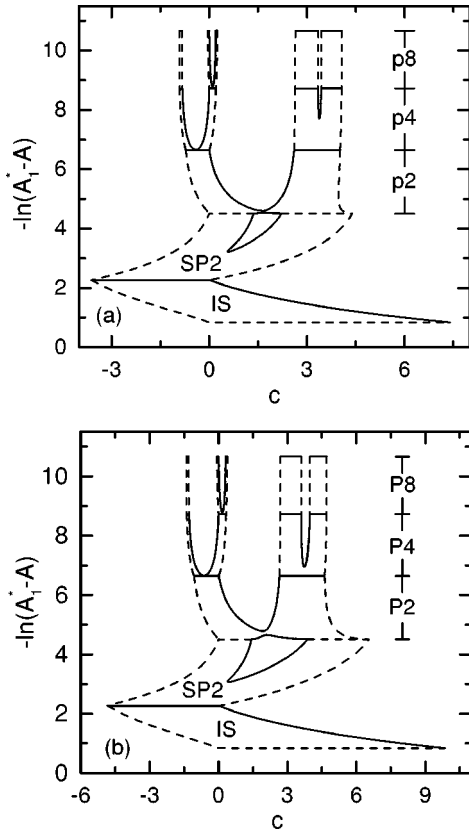


FIG. 7. First stability diagrams of synchronous periodic orbits near the  $c=0$  line for the cases of (a) the quadratic and (b) cubic couplings. Here SP2 and PN ( $N=2, 4$ , and  $8$ ) denote the stable regions of a symmetric orbit of period 2 and an asymmetric orbit with period  $N$ , respectively.

As an example, we consider a linearly coupled, nearest-neighbor coupling case with  $K=1$ , in which the coupling function is

$$g(x_1, \dots, x_N) = \frac{c}{3}(x_2 + x_N - 2x_1) \quad \text{for } N > 3. \quad (39)$$

As shown in Sec. III, the stable region  $U_N$ , in which a synchronous orbit is stable against the perturbations of both modes with indices 0 and  $j$  ( $j \neq 0$ ), varies depending on the mode number  $j$ , because the asynchronous residue  $R_j$  ( $j \neq 0$ ) depends on  $j$ . To find the stability region of the synchronous orbit, one can start with the stability region  $U_G$  for the global-coupling case. Rescaling the coupling parameter  $c$  by a scaling factor  $1/S_N(1, j)$  [ $S_N(K, j)$  is given in Eq. (30)], the stable region  $U_G$  is transformed into a stable region  $U_N(1, j)$ . Then the stability region of the synchronous orbit is given by the intersection of all such stable regions  $U_N$ 's.

As an example, we consider the case with  $N=4$ . Figure 8 shows the stability regions of the synchronous asymmetric  $2^n$ -periodic ( $n=1, 2, 3$ , and  $4$ ) orbits. Note that the scaling factor  $1/S_4(1, j)$  has its minimum value  $\frac{3}{4}$  at  $j=2$ . However, for each synchronous orbit,  $U_4(1, 2)$  itself cannot be the stability region, because bifurcation curves of different modes with nonzero indices intersect one another. We now examine the structure of the stability diagram in Fig. 8, starting from the left side of the stability region of the synchro-

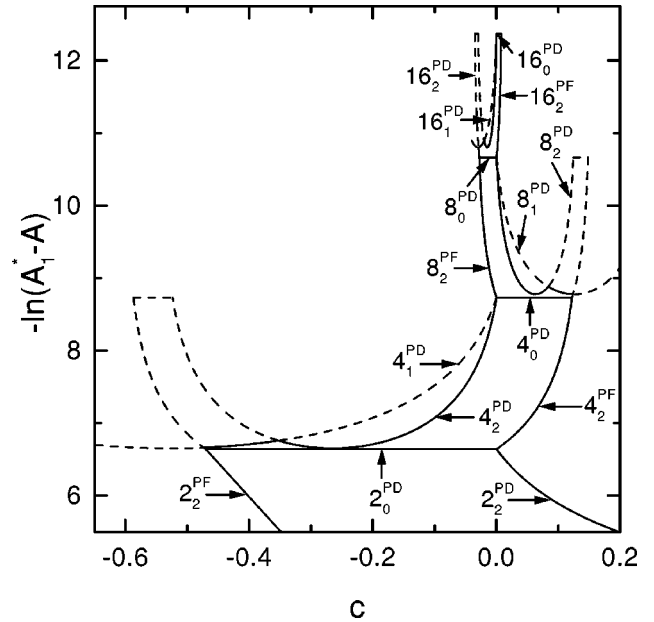


FIG. 8. Stability diagram of synchronous periodic orbits in four linearly coupled inverted pendulums with nearest-neighbor coupling ( $K=1$ ). Each stable region is bounded by its solid boundary curves. For a synchronous orbit of period  $q$ , the PDB (PFB) curve of the mode with index  $j$  is denoted by a symbol  $q_j^{\text{PD(PF)}}$ .

nous asymmetric orbit of level 1 ( $n=1$ ). For the case of level 2 ( $n=2$ ), the zero  $c$  side of  $U_4(1, 2)$ , including a  $c=0$  line segment, remains unchanged, whereas the other side becomes flattened by the bifurcation curve of the asynchronous mode with  $j=1$  [21]. Due to the successive flattening with increasing level  $n$ , a significant change in the stability diagram occurs. Of the infinite number of period-doubling routes for the global-coupling case, only the  $U$  route ending at the zero-coupling critical point remains. Thus only the zero-coupling point is left as a critical point in the parameter plane.

Consider a self-similar sequence of parameters  $(A_n, c_n)$ , at which the synchronous orbit of period  $2^n$  has some given residues, in the  $U$  route for the global-coupling case. Rescaling the coupling parameter with the minimum scaling factor  $1/S_4(1, 2)$  ( $=0.75$ ), the sequence is transformed into a self-similar one for the  $N=4$  case of nearest-neighbor coupling. Hence, the critical behavior near the zero-coupling critical point becomes the same as that for the global-coupling case.

The results for the nearest-neighbor coupling case with  $K=1$  extends to all the other nonglobal-coupling cases with  $1 < K < N/2[(N-1)/2]$  for even (odd)  $N$ . For each nonglobal-coupling case with  $K > 1$ , we first consider a mode with index  $j_{\min}$  for which the scaling factor  $1/S_N(K, j)$  becomes the smallest one and the stability region  $U_N(K, j_{\min})$  including a  $c=0$  line segment. Here the value of  $j_{\min}$  varies depending on the range  $K$ . Like the  $K=1$  case, the zero  $c$  side of  $U_N(K, j_{\min})$  including the  $c=0$  line segment remains unchanged, whereas the other side becomes flattened by the bifurcation curves of the other modes with nonzero indices. Thus the overall shape of the stability diagram of the  $2^n$ -periodic ( $n=1, 2, 3, \dots$ ) orbits born via synchronous supercritical PDB's becomes essentially the same as that for the nearest-neighbor coupling case. Consequently, only the

$U$  route ending at the zero-coupling critical point is left as a period-doubling route, and the critical behavior near the zero-coupling critical point is also the same as that for the global-coupling case.

## V. SUMMARY

The critical behaviors of period doublings in the system of  $N$  symmetrically coupled inverted pendulums have been investigated by varying the two parameters  $A$  and  $c$ . As in the single inverted pendulum [11], the coupled inverted pendulums exhibit multiple period-doubling transitions to chaos with increasing  $A$ . We have studied the first three period-doubling transitions to chaos. For each period-doubling transition to chaos, it has been found that the critical behaviors vary depending on whether or not the coupling is global. For the global-coupling case the zero-coupling critical point and an infinity of critical line segments constitute the same critical set in the  $A$ - $c$  plane, independently of  $N$ . However, for

any other nonglobal-coupling cases the structure of the critical set becomes different from that for the global-coupling case, because of a significant change in the stability diagram of  $2^n$ -periodic orbits ( $n=0,1,2,\dots$ ). The critical scaling behaviors on the critical set have been also found to be the same as those for the abstract system of the coupled 1D maps [14].

## ACKNOWLEDGMENTS

A part of this work had been done while S. Y. K. visited the Center for Nonlinear Studies at the Hong Kong Baptist University. This work was supported by the Basic Science Research Institute Program, Ministry of Education, Korea under Project No. BSRI-97-2401 (S.Y.K.), and in part by grants from the Hong Kong Research Grants Council (RGC) and the Hong Kong Baptist University Faculty Research Grant (FRG).

- 
- [1] R. V. Buskirk and C. Jeffries, *Phys. Rev. A* **31**, 3332 (1985).  
 [2] P. Hadley and M. R. Beasley, *Appl. Phys. Lett.* **50**, 621 (1987); P. Hadley, M. R. Beasley, and K. Wiesenfeld, *Phys. Rev. B* **38**, 8712 (1988).  
 [3] S. H. Strogatz, C. M. Marcus, R. M. Westervelt, and R. E. Mirollo, *Physica D* **36**, 23 (1989).  
 [4] Y. Kuramoto, *Chemical Oscillations, Waves and Turbulence* (Springer-Verlag, New York, 1984).  
 [5] A. T. Winfree, *The Geometry of Biological Time* (Springer-Verlag, Berlin, 1980).  
 [6] L. D. Landau and E. M. Lifshitz, *Mechanics* (Pergamon, New York, 1976), p. 80; V. I. Arnold, *Mathematical Methods of Classical Mechanics* (Springer-Verlag, New York, 1978), p. 113.  
 [7] H. C. Corben and P. Stehle, *Classical Mechanics*, 2nd ed. (Wiley, New York, 1960), p. 67.  
 [8] P. L. Kapitza, in *Collected Papers of P. L. Kapitza*, edited by D. Ter Haar (Pergamon, London, 1965), p. 714.  
 [9] J. J. Stoker, *Nonlinear Vibrations in Mechanical and Electrical Systems* (Interscience, New York, 1966), p. 189.  
 [10] M. Levi, *SIAM (Soc. Ind. Appl. Math.) Rev.* **30**, 639 (1988).  
 [11] S.-Y. Kim and B. Hu, *Phys. Rev. E* **58**, 3028 (1998).  
 [12] M. J. Feigenbaum, *J. Stat. Phys.* **19**, 25 (1978); **21**, 669 (1979).  
 [13] S. Kuznetsov, *Radiophys. Quantum Electron.* **28**, 681 (1985); H. Kook, F. H. Ling, and G. Schmidt, *Phys. Rev. A* **43**, 2700 (1991).  
 [14] S.-Y. Kim and H. Kook, *Phys. Rev. A* **46**, R4467 (1992); *Phys. Lett. A* **178**, 258 (1993); *Phys. Rev. E* **48**, 785 (1993); in *The Proceeding of the First International Workshop on Nonlinear Dynamics and Chaos*, edited by H. Lee (Pohang Institute of Science and Technology, Pohang, Korea, 1993), pp. 49–90.  
 [15] S. Lefschetz, *Differential Equations: Geometric Theory* (Dover, New York, 1977), Sec. 3.5.  
 [16] I. Waller and R. Kapral, *Phys. Rev. A* **30**, 2047 (1984).  
 [17] S. Lefschetz, *Differential Equations: Geometric Theory* (Ref. [15]), p. 60. See Eq. (4.3).  
 [18] S.-Y. Kim and B. Hu, *Phys. Rev. A* **44**, 934 (1991); S.-Y. Kim and D.-S. Lee, *ibid.* **45**, 5480 (1992).  
 [19] J. Guckenheimer and P. Holmes, *Nonlinear Oscillations, Dynamical Systems, and Bifurcations of Vector Fields* (Springer-Verlag, New York, 1983), Sec. 3.5.  
 [20] A. J. Lichtenberg and M. A. Lieberman, *Regular and Stochastic Motion* (Springer-Verlag, New York, 1983), Sec. 5.3.  
 [21] This is also valid for the case of level 1. That is, in the case of level 1 the zero- $c$  left side of  $U_4(1,2)$  remains unchanged, whereas the other right side becomes flattened by the bifurcation curve of the asynchronous mode with  $j=1$ . Consequently, the chimney (consisting of an infinite pile of rectangular-shape regions) in Fig. 2(b) disappears for the nonglobal-coupling case.